Ultrasonic Measurements of Solid Propellant Burning Rates in Nozzleless Rocket Motors

Jean-Claude Traineau* and Paul Kuentzmann†
Office National d'Etudes et de Recherches Aérospatiales, Chatillon, France

Burning rates at several axial locations along the grain port of subscale nozzleless motors were measured by ultrasonic transducers that detect the instantaneous web thickness of the propellant. Two experimental devices were used for this: an axisymmetric nozzleless motor loaded with a metallized composite propellant and a two-dimensional window nozzleless setup loaded with a nonmetallized composite propellant. The ultrasonic transducers give an estimate of the grain deflection during motor pressurization. In both setups, the no-crossflow burning rate measured in the head-end region agrees with standard strand burner data, and high erosive burning rates are found in the aft-end region. These erosive burning data have been represented in a format that includes the main experimental variables: port radius or channel width, no-crossflow burning rate, and mean crossflow velocity. The results reveal that the generally observed trends of threshold specific mass flow rate, no-crossflow burning rate sensitivity, and scale dependence are also demonstrated in nozzleless motors.

Nomenclature

a_o = propellant product head-end sound velocity
A_p = port area
C = sound velocity
C_c = sound velocity in coupling material
C_p = sound velocity in propellant
e_b = propellant web distance burned
e_p = propellant web thickness
k_p = pressure correction coefficient for propellant sound velocity
k_T = temperature correction coefficient for propellant sound velocity
ℓ_p = pressure correction coefficient for coupling material sound velocity
ℓ_T = temperature correction coefficient for coupling material sound velocity
p = static pressure
Q_c = combustion perimeter
R = port radius
T = temperature
T_S = surface temperature of propellant
$\bar{u}$ = mean crossflow velocity
V_C = burning rate
V_{CN} = no-crossflow (or base) burning rate
x = axial distance from motor head-end
α = thermal diffusivity
γ = specific heat ratio
ϵ = erosive burning rate ratio
θ = local slope of burning surface with respect to x axis
$\overline{\rho u}$ = mean specific mass flow rate
ρ_p = solid propellant density
τ = propagation time of ultrasonic waves
τ_o = electronic system time delay

Subscripts

i = denotes initial time conditions (start of test)
f = denotes final time conditions (web burnout)
R = denotes reference conditions

Presented as Paper 84-1469 at the AIAA/ASME/SAE 20th Joint Propulsion Conference, Cincinnati, OH, June 11-13, 1984; received Oct. 4, 1984; revision received Dec. 10, 1985.

*Research Engineer, Chemical Propulsion Division.
†Head, Chemical Propulsion Division.

Introduction

WITHIN the framework of integral-rocket-ramjet missile systems, studies have been conducted on nozzleless motors since 1978 in France by Société Nationale des Poudres et Explosifs (SNPE) and Office national d'Etude et de Recherches Aérospahales (ONERA). These studies have led to a simple first generation program[1] that gives an a priori prediction accurate to within ±5% of total perfomance if a realistic data base is available (thermodynamical properties of combustion products, no-crossflow and erosive burning rates in the whole pressure range).

A survey of the technology literature gives a good idea of how difficult it is to improve the accuracy of this prediction. Procinsky[2] has given a complete list of the main phenomena that have to be studied and the major modifications that have to be carried out before a program can be used to predict the performance of a completely new design.

Among the numerous problems listed by Procinsky is the prediction of the no-crossflow and erosive burning rates of the propellant. King[3-5] has developed a specific calculation module for predicting the propellant burning rate in nozzleless motors as a function of pressure and crossflow velocity. This module contains five options for the calculation of the steady-state burning rate. Only the first is based on correlation of calculations made using King's erosive burning model for composite AP propellants. The other options need at least tables of no-crossflow burning rate and tables of the erosive ratio V_C/V_{CN} vs pressure and crossflow velocity for a given channel diameter.

To fill these tables, many results devoted to the driver/sample technique or to simulative studies may be found (i.e., Marklund and Lake,[6] Razdan and Kuo,[7] King,[8] Dunlap et al.,[9] Yamada et al.[10]) but there is no work that reports measurements of burning rates in a nozzleless booster directly. According to the widely accepted assumption that erosive burning is due to the enhancement of transport properties by crossflow generated turbulence in the flame zone,[11] a theoretical fluid dynamics model is required to relate this wide data base and the erosive burning in the motor. Such a model is not yet achieved, in spite of some advanced works in this area.[12-14] Therefore, experiments on actual motors with direct measurements of burning rate remain very useful.

Among the direct burning rate measurement methods developed during the last ten years, the microwave technique is probably the most attractive.[15] Measurements are already

available for samples mounted in a waveguide, and application only to small grains is foreseen in the near future.[16] Thus this technique cannot yet be used for direct measurements in actual motors. Since 1973, experience in the ultrasonic technique acquired at ONERA has been used for measuring burning rates with satisfactory results in steady or slowly varying conditions on composite, double-base, or self-pyrolyzing propellants. This method has been applied to subscale nozzleless motors and realistic burning rate data have been obtained. The principle of the measurement method and its data processing is first summarized in this paper, a description of the two experimental setups is then given, and the most characteristic results obtained to date are described.

The Ultrasonic Method

Principle of the Method

The principle of the method is the following: a mechanical wave emitted by a transducer travels through the propellant, reflects off the grain surface because of the large difference in acoustic impedance between propellant and combustion products, and comes back to the transducer. The measurement of the propagation time of a pulse is related to the propellant web thickness and the burning rate is thus deduced by differentiation.

Selecting and Mounting the Transducer

Specific tests, performed at ONERA since 1974, have taught the following main lessons:

1) The propagation velocity of ultrasonic waves in propellants at room temperature lies between 1750 and 1900 m/s and gives a propagation time of about 30 μs for a 30-mm propellant web thickness. A broad bandwidth can thus be expected for the system.

2) The sound damping in solid propellants at ultrasonic frequencies is noticeably higher than the damping in the audible frequency range and limits the propellant web thickness that can be measured to about 40 mm for a typical composite propellant.

3) Optimization of the transducer characteristics has led to the choice of transducers working around 2.25 MHz for three different diameters (1, ¾, and ½ in.), which allows a good adaptation to the various grain geometries tested.

4) The introduction of an intermediary coupling element between transducer and propellant is necessary to give a quasilinear operation down to zero propellant web thickness, to reduce transducer damping problems and near field effects, and to completely insulate the transducer from the severe pressure and temperature conditions prevailing in the combustion chamber.

The coupling material must have an acoustic impedance as close as possible to that of the propellant, low ultrasonic damping, good mechnical strength, and perfect binding to the propellant. For an AP/polybutadiene/Al composite propellant, a hardening castable epoxy resin, loaded or not with pulverized silica, has these characteristics.

Implementation of the ultrasonic transducer in a simple setup with a small end burning grain is displayed in Fig. 1. In this setup, which is used to determine the base burning rates and the L* instability map of a propellant, the burning surface remains flat during burn time. Recent tests have also shown that ultrasonic emission and reception can be used on an axisymmetric grain with a cylindrical port, because the propagation properties of the propellant induce a very directive acoustic field. Therefore there is no influence of the port curvature and the measurement is precisely located.

First Data Processing Method and Results

Kuentzmann et al.[17] have given a detailed description of how the ultrasonic transducer must be fitted and of the electronic propagation time measuring device. The first data processing method is based on the assumption that the sound velocity is constant in both the propellant and the coupling material. Once the propagation time is known, the propellant web thickness is simply deduced from the equation:

$$\tau = \tau_o + 2(e_c/C_c) + 2(e_p/C_p) \tag{1}$$

Following this major assumption, numerous tests have been performed on composite propellants, double-base propellants, and self-pyrolyzing fuels. The results have demonstrated that the method is at least as accurate as more classical methods and is able to determine quasisteady burning rate curves over wide pressure ranges in a single test. However, for unsteady burning rates, or tests with fast pressure variations, this easy procedure seems to be inadequate. Cauty[18] has shown that sound velocity is sensitive to pressure and temperature. These influences have been demonstrated experimentally, and the following relation between pressure, temperature, and sound velocity has been deduced:

$$C_R/C = [1 - k_p(p - p_R)]\,[1 + k_T(T - T_R)] \tag{2}$$

This leads to a new data processing method, which appears necessary if the accuracy of the method is to be increased for any kind of test condition, and particularly for nozzleless motor tests.

New Data Processing Method

The system considered is made of an ultrasonic transducer, in contact with the coupling element, itself bonded to the propellant as shown in Fig. 2.

One takes into account the fact that the propagation velocities in both the propellant and coupling material are unique functions of local pressure and temperature. The electronic device monitored by a minicomputer gives propagation time measurements at a rate of about 5000 Hz. This propagation time can be expressed as

$$\tau = \tau_o + 2\int_{x_S}^{x_I} \frac{dx}{C_p(T,p)} + 2\int_{x_I}^{x_T} \frac{dx}{C_c(T,p)} \tag{3}$$

Assuming that pressure is uniform and equal to the combustion chamber pressure and the temperature of the coupling

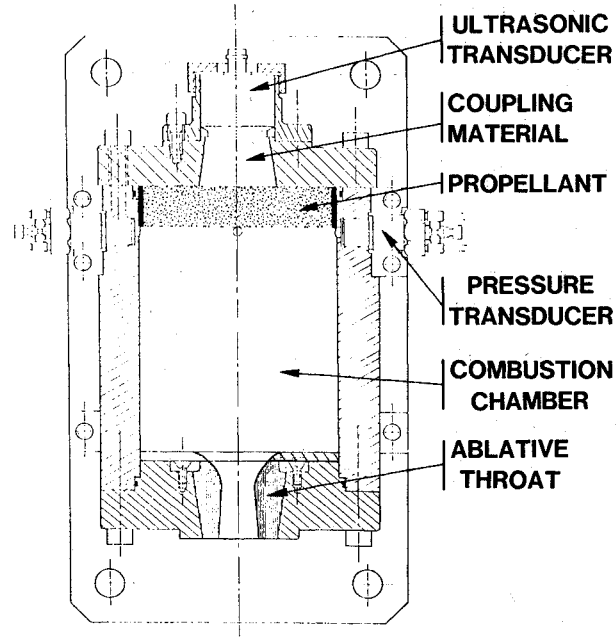

Fig. 1 Schematic of a simple setup fitted with an ultrasonic transducer.

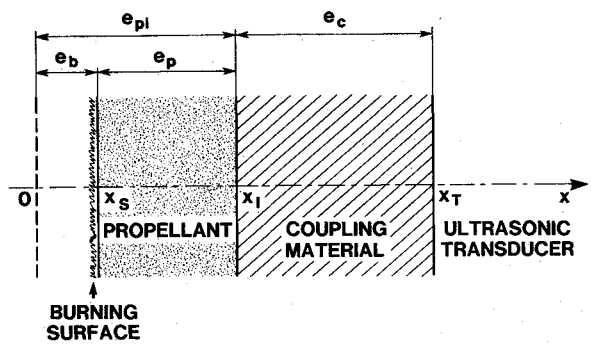

Fig. 2 Definition of the system parameters.

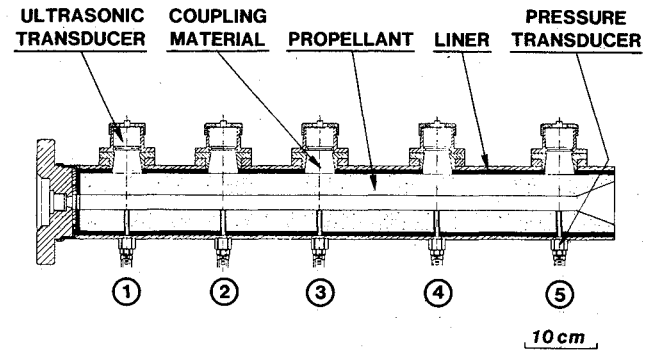

Fig. 3 Cross section of the axisymmetric nozzleless motor.

material remains at its initial value, Eq. (3) simplifies to

$$\tau=\tau_o+2\int_{x_S}^{x_I}\frac{dx}{C_p(T,p)}+\frac{2e_c}{C_c(T_i,p)} \tag{4}$$

In particular, when the propellant web thickness is down to zero (web burnout), one can write

$$\tau_f=\tau_o+\frac{2e_c}{C_c(T_i,p_f)} \tag{5}$$

Eliminating τ_o between Eqs. (4) and (5) yields

$$\tau-\tau_f=2\int_{x_S}^{x_I}\frac{dx}{C_p(T,p)}+\frac{2e_c}{C_c(T_i,p)}-\frac{2e_c}{C_c(T_i,p_f)} \tag{6}$$

Using Eq. (2) for the propellant and the coupling material, Eq. (6) becomes

$$\tau-\tau_f=\frac{2[1-k_p(p-p_R)]}{C_{pR}}\int_{x_S}^{x_I}[1+k_T(T-T_R)]dx$$
$$+\frac{2e_c}{C_{cR}}[1+1_T(T-T_R)]1_p(p-p_f) \tag{7}$$

In the case of steady-state combustion, the expression for the temperature profile in the propellant is usually given by

$$T-T_i=(T_S-T_i)\exp[-V_C(x-x_S)/\alpha] \tag{8}$$

With this formula, Eq. (7) yields:

$$\tau-\tau_f=\frac{2[1-k_p(p-p_R)]}{C_{pR}}\{[1+k_T(T_i-T_R)]e_p$$
$$+k_T(T_S-T_i)\frac{\alpha}{V_C}[1-\exp(-V_Ce_p/\alpha)]\}$$
$$+\frac{2e_c}{C_{cR}}[1+1_T(T-T_R)]1_p(p-p_f) \tag{9}$$

Using the current values for α, e_p and V_C, one can neglect $\exp(-V_Ce_p/\alpha)$ compared to unity to get

$$\tau-\tau_f=\frac{2[1-k_p(p-p_R)]}{C_{pR}}\left\{[1+k_T(T_i-T_R)]e_p\right.$$
$$\left.+k_T(T_S-T_i)\frac{\alpha}{V_C}\right\}+\frac{2e_c}{C_{cR}}[1+1_T(T-T_R)]1_p(p-p_f) \tag{10}$$

At this point of the processing, the different terms have to be evaluated. For AP/polybutadiene composite propellants, average values of the correction coefficients are (results experimentally found by Cauty[18]) for the propellant: $k_p\simeq 3\times10^{-9}\text{Pa}^{-1}$, $k_T\simeq 2.9\times10^{-3}\text{K}^{-1}$, and for the coupling material: $1_p\simeq 0.5\times10^{-9}\text{Pa}^{-1}$, $1_T\simeq 2.5\times10^{-3}\text{K}^{-1}$.

With the above value for the temperature correction coefficient for the propellant sound velocity, the expression between brackets in Eq. (10) can be approximated by $[1+k_T(T_i-T_R)]e_p$, within 0.2% relative error. This approximation amounts to disregarding the effect of the temperature profile in the propellant and thus assumes that the entire propellant can be taken as being at its initial temperature.

Hence, one obtains from Eq. (10) the instantaneous web distance burned

$$e_b=e_{pi}-\left[\frac{C_{pR}}{2}(T-T_f)-\frac{C_{pR}}{C_{cR}}1_p(p_f-p)e_p\right]\Big/[1-k_p(p-p_i)] \tag{11}$$

where the initial and reference conditions are room conditions. This final expression completely defines the instantaneous web distance burned as a function of propagation time and pressure and is the one used in the data processing method.

Experimental Test Apparatuses

The measurement of burning rates in nozzleless motors is one part of studies whose objectives were to determine the effects of grain geometry on performance, assess reproducibility, and visualize the grain regression for correlation with computation. To this end, two experimental test apparatuses have been designed, constructed, and checked out.

The first apparatus is an axisymmetric subscale nozzleless motor with an AP/CTPB/Al composite propellant. Ten tests have been successfully carried out using two length-to-diameter ratios (L/D), and, therefore, two different operating pressure ranges. The main results concerning erosive burning have been deduced from the higher L/D ratio motor which is shown schematically in Fig. 3. This figure also illustrates the implementation of an ultrasonic transducer on this axisymmetric grain. Five stations for measuring static pressure and web thickness are located along the grain. A classical exit cone is machined into the aft-end to prevent break-off from the end of the grain and to increase performance by recovery of kinetic energy.[19]

The second experimental setup is a laboratory device with two slabs of propellant simulating a two-dimensional nozzleless motor. High speed motion-picture cameras give the evolution of the burning surface through a single plexiglass window that covers the total grain length. To reduce flame temperature effects, an AP/HTPB nonmetallized composite propellant has been chosen. A schematic of this apparatus, which is presented in Fig. 4, shows the numerous static pressure measurements along the channel, the diverging section of the grain, and the two ultrasonic transducer locations. Table 1 gives the grain configuration and defines the propellant for each experimental setup. In both cases, the igniter is a microrocket at the head-end of the port, which provides reproducible results and is easy to model in a computer program.

Before going into the data processing method, an interesting piece of information should first be noted. It comes from the port photographs taken during a two-dimensional test. Figure 5 gives an idea of the grain burnback in the aft-end region: the first and the second pictures concern the start and the end of the stabilized phase of the test, respectively. They show that the evolution of port geometry gradually leads to a narrowing of the "throat" section, due to the axial pressure gradient effects. These observations are very useful to correlate computed burnback in this region, which is directly related to the accuracy of performance prediction programs.

Results

Data Processing and Preliminary Results

Data processing starts with the computation of pressure at each measurement location, using a calibration curve and correcting any thermal drift. Curves of the five axial pressures vs time are given in Fig. 6 for one of the axisymmetric motor tests. One will observe the high initial pressure peak and fast decrease of the curves, aggravated by the presence of erosive burning. The incident located at 1.9 s remains unexplained but has no influence on the erosive range, which is limited to about the first one-and-one-half seconds of the test.

Figure 7 shows four of the basic pressure curves for a two-dimensional test and gives a good idea of the large axial pressure differential between head-end and aft-end of a

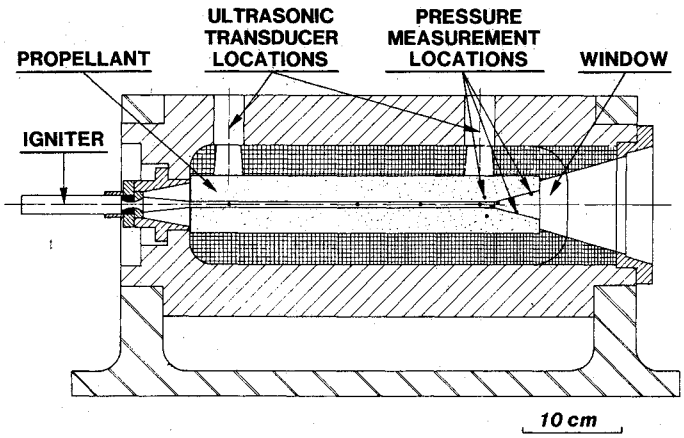

Fig. 4 Cross section of the two-dimensional setup.

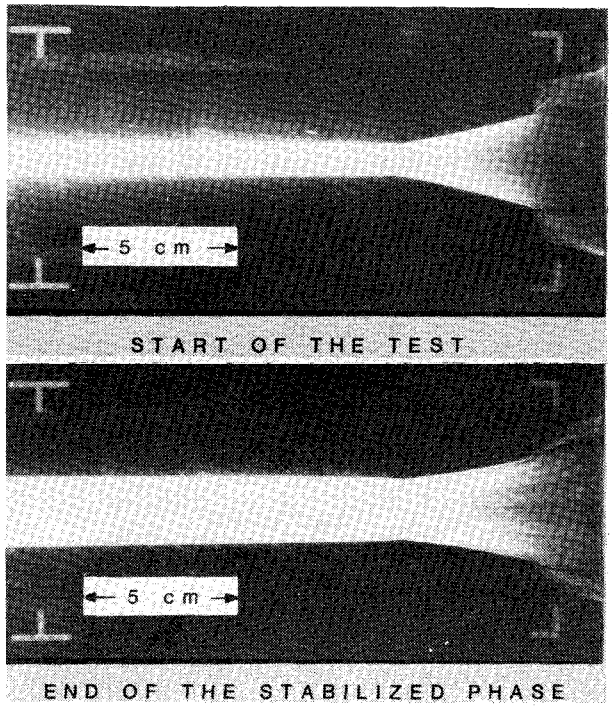

Fig. 5 Evolution of the aft-end port geometry during a two-dimensional test.

Table 1 Setup configurations

Setup	Grain configuration		Propellant
I	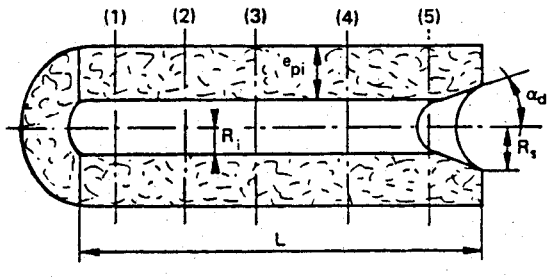 Cylindrical with exit cone	length L = 750 mm initial port radius R_i = 10 mm initial web thickness e_{pi} = 30 mm exit cone radius R_s = 30 mm exit cone angle α_d = 20° Measurement locations : x_1 = 70 mm, x_2 = 200 mm, x_3 = 330 mm, x_4 = 475 or 500 mm, x_5 = 650 or 675 mm, } from the head-end	70/14/16 AP/CTPB/Al, ≅ 90 μm AP a_0 ≃ 1070 m/s γ ≃ 1.135
II	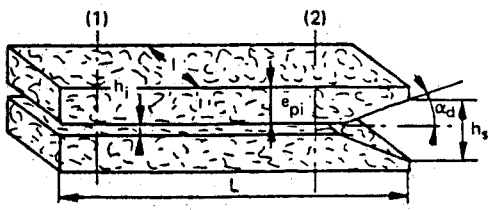 Two-dimensional with simulated diverging section	length L = 345 mm initial port section area h_i = 6 mm, l = 40 mm initial web thickness e_{pi} = 25 mm exit section height h_s ≈ 30 mm exit section angle α_d = 15° Measurement locations : x_1 = 35 mm, x_2 = 285 mm, } from the head-end	85/15 AP/HTPB combustion modified ≃ 200 μm AP a_0 ≅ 1090 m/s γ = 1.2

nozzleless motor. It can be noted that this pressure differential effect decreases with time. This is demonstrated by the pressures at the 300 and 305 mm axial stations, respectively located just upstream and downstream of the "throat" section. These pressures are clearly different at the start of the test and tend to merge gradually during web time. One will also notice that premature extinction, associated with bulk-mode instabilities[20] due to the fast decrease of the pressure, occurs at 0.86 s when only 40% of the web thickness has been burned.

The web distance burned at each measurement station is calculated from the propagation time using Eq. (11). The pressure correction coefficients for the propellant and coupling material sound velocities that appear in this formula are assumed to be known from other tests. Figure 8 shows a set of results obtained in the two-dimensional setup near the head-end and aft-end regions of the grain. This figure calls for the following remarks: 1) The web distance burned varies greatly from the head-end to the aft-end because of the burning rate sensitivity to local pressure and crossflow velocity. 2) A detailed view of the early stage of the test reveals an abnormally fast evolution of the web distance burned in the aft-end region during the transient pressure phase, while the head-end region seems to burn quite normally. This sharp rise, which reaches almost 0.5 mm, may have three different causes: 1) The effect of pressure variations on the ultrasonic measurement, 2) extra burning rate during transient phase, and 3) grain deflection during motor pressurization. The first cause must be eliminated because the effect of pressure variations on the ultrasonic measurements is taken into account and corrected by means of the pressure correction coefficient. Differentiating between the last two causes can be illustrated by the axisymmetric nozzleless motor test results. In Fig. 9, for each axial measurement location, the web distance during ignition is plotted (open circles) vs the distance from the head-end. At location 1 near the head-end, the measured web distance burned is compared to the estimated normal web distance burned during ignition (black triangle), which is calculated by the integration of the quasisteady-state burning rate. The stated discrepancy between these two values can be partially attributed to transient combustion effects, but the major part of it is probably due to the grain deflection. Thus, the curve drawn gives an idea of the deformed grain contour during motor pressurization. This deformed contour appears realistic for such a case-bonded nozzleless grain. The contour also agrees with the trends given by the NPP grain deflection model,[21] i.e., limited deflections in the head-end region and large axial and radial deflections in the exit-cone area.

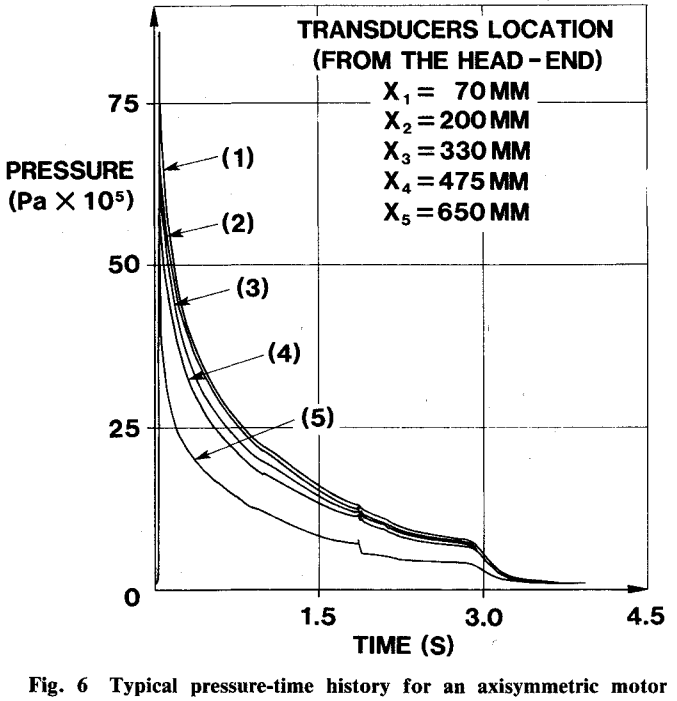

Fig. 6 Typical pressure-time history for an axisymmetric motor test.

Burning Rate Results

Translation from sampled web distances burned to burning rates requires a numerical differentiation. It is well known that this kind of operation is one of the most unstable. Thus, one proceeds by eliminating outlying data, performing least square line regression on 201 data points and computing the central value, smoothing these central values by the "ordinate regularization" method,[22] numerically differentiating on 3 or 5 resulting points, and smoothing the derivatives. This method is certainly not optimal, but it reduces operator intervention to the choice of only one smoothing coefficient. All these operations are computerized and a plotting program then allows a systematic exploitation of results. It must be noted here that this differentiation does not give the real burning rate V_C, but the projection of V_C on the transducer axis, i.e., $V_C\cos\theta$. However, in typical configurations θ remains small and the experimental measurement is assumed to be the actual burning rate V_C.

Typical results are presented in Fig. 10 (axisymmetric motor) and Fig. 11 (two-dimensional setup) by means of burning rate curves as functions of pressure. In Fig. 10, the five curves obtained from the five ultrasonic transducers are

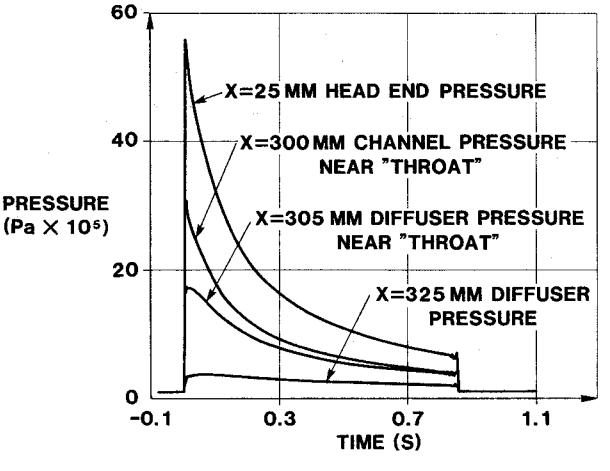

Fig. 7 Four basic pressure curves for a two-dimensional test.

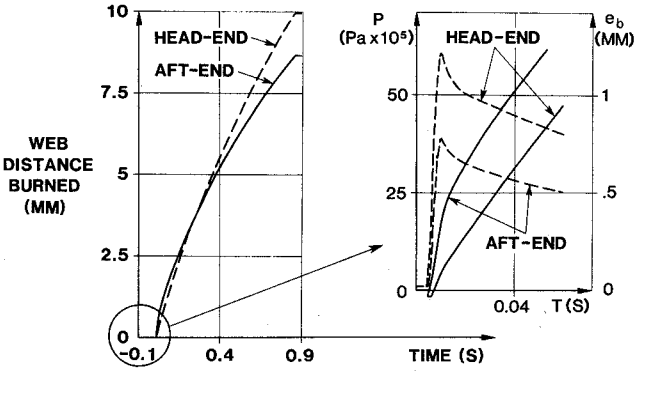

Fig. 8 Comparison between head-end and aft-end ultrasonic measurements for a two-dimensional test.

drawn. One observes the good agreement of the measurements in the head-end region (locations 1 and 2). Moreover, the comparison shows an increasing discrepancy between the curves proceeding from the head-end to the off-end regions. This discrepancy expresses the erosive combustion phenomenon which, for this test, leads to a departure from the base burning rate that reaches a maximum of 65% at location 5, under a pressure of 30×10^5 Pa. The well known threshold effect is here brought to light. Below the erosive burning threshold, curves agree to the nearest measurement dispersion. In the second experimental apparatus, similar results can be noted (Fig. 11) with an extra burning rate which reaches 55% at location 2 under a pressure of 32×10^5 Pa.

The reliability of the method and the reproducibility of its results are demonstrated in Fig. 12. In this figure, two identical axisymmetric tests are compared to classical strand burner data. These results indicate that under nonerosive conditions, the motor results are in good agreement with strand burner data and show little scatter; and reproducibility of erosive combustion at location 5 is also rather good, particularly if one takes into account a small change in transducer location between the two tests (650 and 675 mm).

Displaying the Erosive Phenomenon

There is no one way to present erosive burning data. One can, for example, use the classical erosive burning rate ratio:

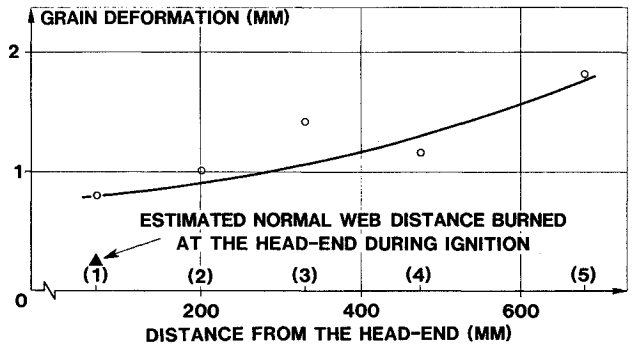

Fig. 9 Estimation of the deformed grain contour deduced from ultrasonic measurements during pressurization of an axisymmetric motor test.

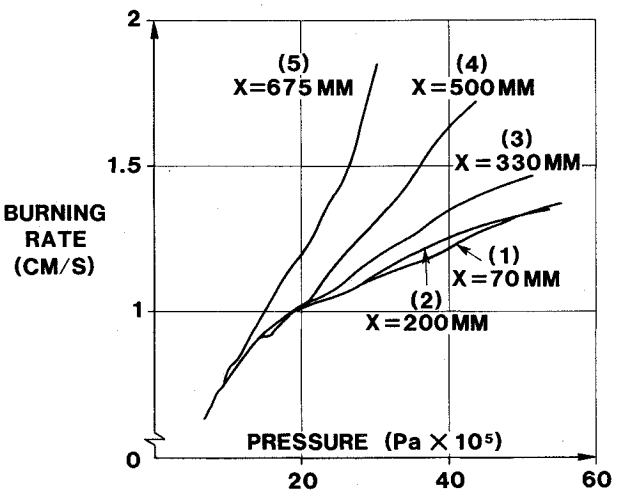

Fig. 10 Complete results of ultrasonic burning rate measurements for an axisymmetric motor test.

$\epsilon = V_C/V_{CN}$ as a function of the specific mass flow rate. The experimental data are sufficient to compute at any time and at each measurement station a mean specific mass flow rate ρu by a numerical approximation of the integral:

$$\overline{\rho u} = \frac{1}{A_p}\int_0^x \frac{Q_C V_C \rho_p dx}{\cos\theta} \simeq \frac{1}{A_p}\int_0^x Q_C V_C \rho_p dx \qquad (12)$$

Furthermore, at any pressure, the burning rate curve 1 on Fig. 10 can be used to extrapolate the base burning rate V_{CN} for each measurement location. Fig. 13 shows a set of results from one of the axisymmetric motor tests for the last three measurement stations 3, 4, and 5. This figure clearly displays the generally observed phenomenon of threshold specific mass flow rate. However, this mode of representation is not exempt from criticism because the evolutions of pressure and port radius, which are important in the case of a nozzleless motor, are hidden. Thus, it is necessary to select a better way of representation.

It is reasonable to assume that ϵ, in the steady-state case, depends on three main quantities. The first is specific to the base burning. V_{CN} can be selected because it is experimentally known and leads to an efficient flame height by way of a calculation model. The second characterizes geometry. The local port radius must obviously be chosen. The last represents the flow. The choice of this third parameter depends on the description used to depict the flow.

Taking a local value of the flow as $\tilde{u}$ or $\overline{\rho u}$ goes along with a one-dimensional description, which is the easiest flow representation. However, this assumption implies that the upstream portion of the flow has negligible influence on local erosive burning. In spite of this reservation, the mean crossflow velocity $\tilde{u}$ has been selected in order to compare these results with previous works. Considering a constant enthalpy flow, we easily arrive at:

$$\tilde{u} = \frac{2a_o B}{\gamma + \sqrt{\gamma^2 + 2(\gamma-1)B^2}} \quad \text{where} \quad B = \frac{\overline{\rho u} a_0}{p} \qquad (13)$$

This formula requires only a_o and γ, which are supposed to be known with enough accuracy.

Within the framework of nozzleless motors and one-dimensional flows, the local Mach number is, in a first ap-

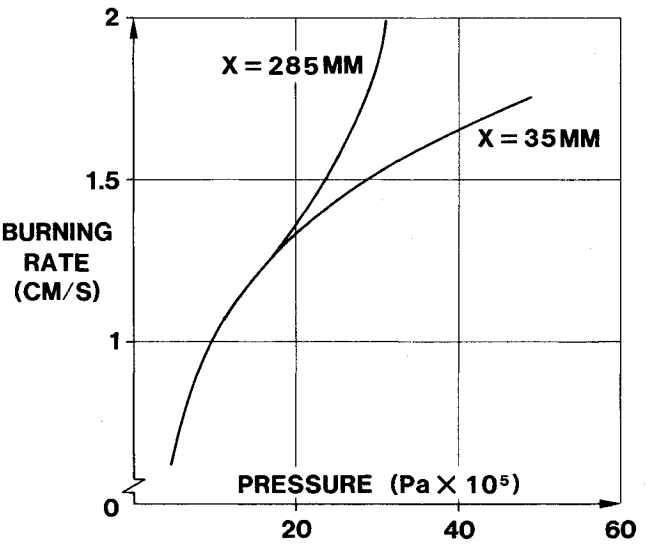

Fig. 11 Complete results of ultrasonic burning rate measurements for a two-dimensional test.

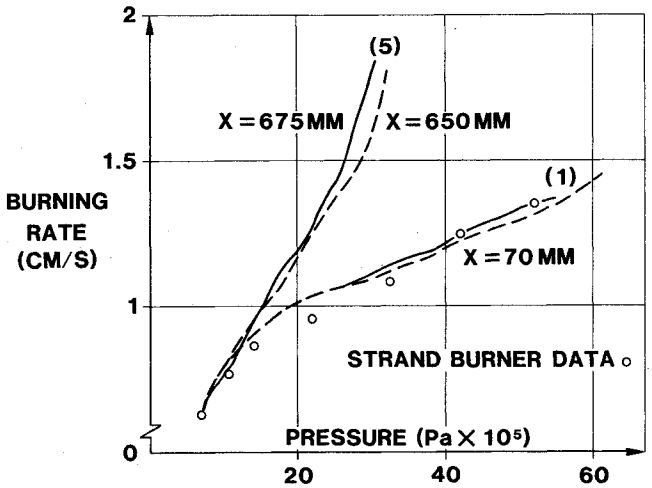

Fig. 12 Reproducibility of ultrasonic burning rate measurements and comparison with strand burner data.

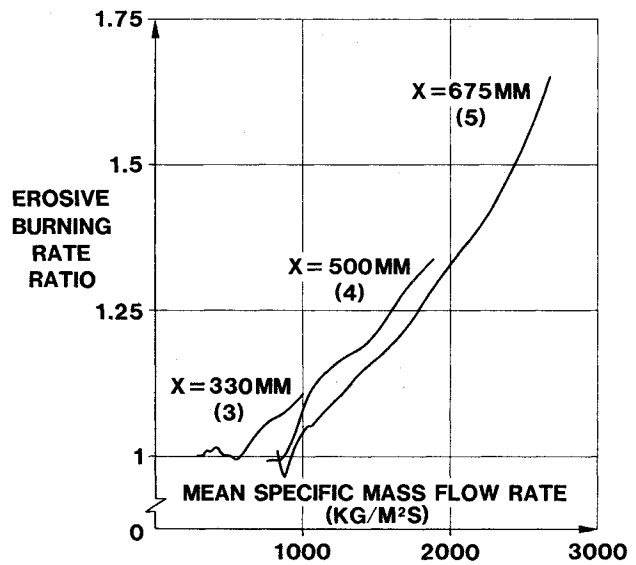

Fig. 13 Typical erosive burning results representation for an axisymmetric motor test.

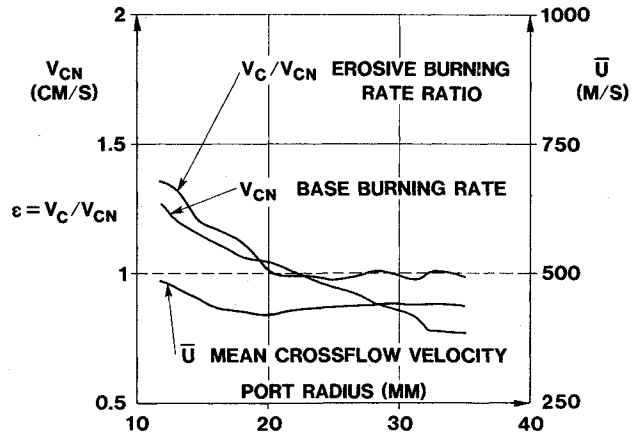

Fig. 14 Erosive burning results at location 4 (500 mm from the head-end) during an axisymmetric motor test.

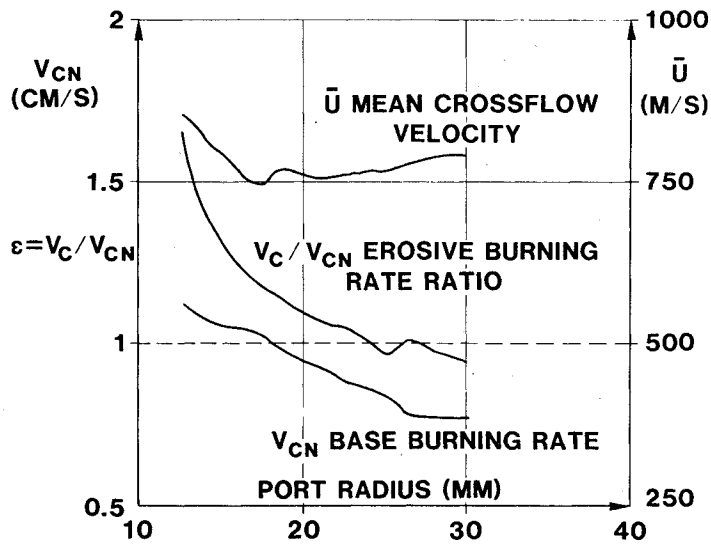

Fig. 15 Erosive burning results at location 5 (675 mm from the head-end) during an axisymmetric motor test.

proximation, closely related to the axial distance from the motor head-end divided by the channel length. In this kind of test, the mean crossflow velocity at a given station is a priori almost independent of time and cannot be taken as a main parameter. If one keeps the combustion quantities V_{CN} and ϵ as unknowns, the only remaining parameter is the port radius. This parameter also has the advantage of varying monotonously with time. It is thus logical to plot ϵ, V_{CN}, and $\bar{u}$ as functions of R at each location.

Figures 14 and 15 illustrate results obtained during the same test at the two aft-end locations of the axisymmetric motor. One observes small oscillations which have no physical meaning but are related to the data processing method. The mean crossflow velocity is not strictly constant because of the nonlinear grain burnback due to the differential effects of burning rates along the grain.

To carry out a synthesis of the results obtained by different tests at the two aft-end locations, a format that includes the main experimental variables has to be chosen. A representation of the erosive burning rate ratio vs mean crossflow velocity, for values of port radius between 13 and 20 mm and a no-crossflow burning rate between 0.93 and 1.1 cm/s has been selected and is displayed in Fig. 16. Such a representation is insufficient to define the complete erosive burning behavior of a given propellant in nozzleless rocket configurations because the influence of the upstream portion of the flow at each measurement location is not taken into account. However, these results confirm the combined influences, previously demonstrated by King,[3] of flow ($\bar{u}$), combustion (V_{CN}), and geometry (R) on nozzleless erosive burning sensitivity.

One can try to separate each of these effects and compare the trends with those deduced from driver/sample technique tests:[6-8] At constant R (i.e., 15.2 mm), erosive burning decreases with increasing no-crossflow burning rate ($\epsilon = 1.27$ for $V_{CN} = 1.05$ cm/s and $\epsilon = 1.19$ for $V_{CN} = 1.1$ cm/s). At constant V_{CN} (i.e., 1.1 cm/s), a narrow cross-sectional area exhibits greater trend toward erosion than a larger cross-sectional area ($\epsilon = 1.55$ for $R = 13$ mm and $\epsilon = 1.05$ for $R = 17$ mm). These results are found to be in agreement with the generally observed scale dependence and no-crossflow burning rate sensitivity.

The work in order now is to correlate this new data base with theoretical results obtained by the ONERA erosive burning program. This program is based on the assumption that erosive burning is due to turbulence penetrating the flame zone. It solves the two-dimensional steady-state Navier-Stokes equations by means of the numerical technique proposed by Patankar and Spalding.[23] For the closure of the problem, a modified Prandtl mixing length approach for the turbulent viscosity is used in the boundary layer, and Couette equations are integrated in the vicinity of the burn-

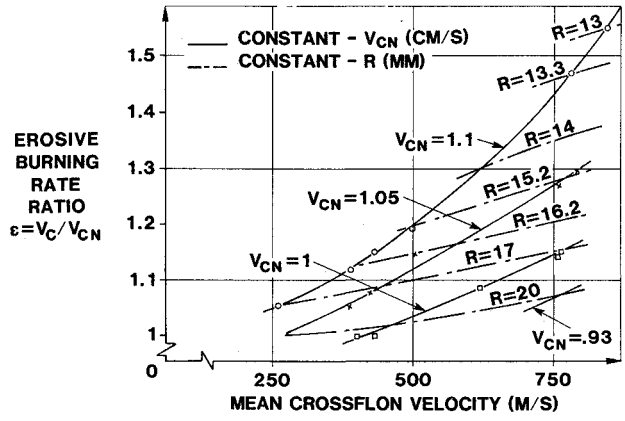

Fig. 16 Synthesis of the erosive burning results for the axisymmetric motor tests.

ing surface. Two sets of computer runs are scheduled. The first one, which will use the complete experimental burning rate distribution, is intended to validate the program in nozzleless conditions and to give the axial velocity profile evolution along the port. The second one, without experimental data input, aims at giving an a priori prediction of erosive burning to be compared with the present experimental results.

Conclusion

The ultrasonic measurement method has been applied to erosive burning rate measurements in two subscale nozzleless motors and original results have been obtained under realistic operating conditions. Complementary information concerning nozzleless motor grain deflection during ignition has also been deduced from the ultrasonic measurements. At the present time, the ultrasonic technique seems to be well suited to such a task, if one limits investigations to quasi-steady-state combustion regime.

A single test gives sufficient data to compute the whole no-crossflow burning rate law and erosive components for various values of the mean flow velocity for a wide range of pressure and several dimensions of the port. Comparison with standard strand burner data in nonerosive conditions has proven that data scattering is reduced enough to attribute a good degree of confidence to these results.

For nozzleless motor tests, depicting erosive burning rate results in a form that includes the principal experimental variables is not an easy task because of the combined effects of flow, combustion, and geometry. A representation of the erosive burning rate ratio vs mean crossflow velocity for different values of port radius and no-crossflow burning rate has been chosen. Such a representation in terms of local parameters is insufficient to define the erosive burning behavior of a given propellant in nozzleless rocket motor applications because the history of the flow is not taken into account. However, the results are found to be in agreement with the main trends as they are generally observed and predicted by current models for erosive burning. Work is in progress to complete the synthesis of experimental information and to interpret this erosive burning data base by further modeling. It can be thought that these recent data will allow a better definition of the appropriate model to be used to predict nozzleless motor performance in greater detail. Although nozzleless motors have specific applications, this topic remains of scientific interest, essentially because it implies a complete control of the solid propellant combustion.

Acknowledgments

This research was sponsored by the Direction des Recherches, Etudes et Techniques, Délégation Générale pour l'Armement under contracts 82.34.111 and 83.34.134. The authors are grateful to SNPE for manufacturing the propellant grains.

References

[1]Nahon, S., "Nozzleless Solid Propellant Rocket Motors—Experimental and Theoretical Investigations," AIAA Paper 84-1312, June 1984.

[2]Procinsky, I.M. and Yezzi, C.A., "Nozzleless Performance Program," AIAA Paper 82-1198, June 1982.

[3]King, M.K., "Prediction of Solid Propellant Burning Rates in Nozzleless Motors," AIAA Paper 82-1200, June 1982.

[4]King, M.K., "A Model of Erosive Burning of Composite Propellants," *Journal of Spacecraft and Rockets*, Vol. 15, June-July 1978, pp. 139-146.

[5]King, M.K., "A Model for the Effects of Pressure and Crossflow Velocity on Composite Propellant Burning Rate," AIAA Paper 79-1171, June 1979.

[6]Marklund, T. and Lake, A., "Experimental Investigation of Propellant Erosion," *American Rocket Society Journal*, Vol. 30, Feb. 1960, pp. 173-178.

[7]Razdan, M.K. and Kuo, K.K., "Measurements and Model Validation for Composite Propellants Burning Under Crossflow of Gases," *AIAA Journal*, Vol. 18, June 1980, pp. 669-677.

[8]King, M.K., "Erosive Burning of Composite Solid Propellants: Experimental and Modeling Studies," *Journal of Spacecraft and Rockets*, Vol. 16, June-July 1979, pp. 154-162.

[9]Dunlap, R., Willoughby, P.G., and Hermsen, R.W., "Flowfield in the Combustion Chamber of a Solid Propellant Rocket Motor," *AIAA Journal*, Vol. 12, Oct. 1974, pp. 1440-1442.

[10]Yamada, K., Goto, M., and Ishikawa, N., "Simulative Study on the Erosive Burning of Solid Rocket Motors," *AIAA Journal*, Vol. 14, Sept. 1976, pp. 1170-1177.

[11]Lengellé, G., "Model Describing the Erosive Combustion and Velocity Response of Composite Propellants," *AIAA Journal*, Vol. 13, March 1975, pp. 315-322.

[12]Beddini, R., "Reacting Turbulent Boundary-Layer Approach to Solid Propellant Erosive Burning," *AIAA Journal*, Vol. 16, Sept. 1978, pp. 898-905.

[13]Beddini, R., "Analysis of Injection-Induced Flows in Porous-Walled Ducts with Application to the Aerothermochemistry of Solid Propellant Motors," Ph.D. Rutgers, The State University of New Jersey, New Brunswick, NJ, 1981.

[14]Godon, J-C., "Modélisation de la combustion normale et érosive des propergols composites," These de Doctorat d'Etat, Université Pierre et Marie Curie, Paris, France, 1983.

[15]Strand, L.D., Magiawala, K.R., and McNamara, R.P., "Microwave Measurements of Solid Propellant Pressure-coupled Response Function," AIAA Paper 79-1211, June 1979.

[16]Mathes, H.B. and Battles, J.W., "A 35 Gigahertz System for Measurement of Solid Propellant Acoustic Combustion Response," *Proceedings of the 18th JANNAF Combustion Meeting*, Pasadena, CA, CPIA Pub. 347, Vol. III, Oct. 1981, pp. 161-165.

[17]Kuentzmann, P., Demarais, J.C., and Cauty, F., "Mesure de la vitesse de combustion des propergols solides par ultrasons," *La Recherche Aérospatiale*, Vol. 1, Jan.-Feb. 1979, pp. 55-72.

[18]Cauty, F., "Mesure par ultrasons de la vitesse de combustion des propergols solides," Mémoire CNAM, Paris, 1983.

[19]Procinsky, I.M. and McHale, C.A., "Nozzleless Boosters for Integral-Rocket-Ramjet Missile Systems," *Journal of Spacecraft and Rockets*, Vol. 18, June-July 1981, pp. 193-199.

[20]Thrasher, D.I., "Bulk-Mode Instability of Nozzleless Rocket Motor," *Proceedings of 9th JANNAF Combustion Meeting*, Monterey, CA, CPIA Pub. 231, Vol. I, 1972, pp. 35-47.

[21]Murray, J.W., Mikeska, A.J., and Tonkin, M.E., "NPP Grain Deflection Model," AIAA Paper 82-1201, June 1982.

[22]Coulmy, G., "Exploitation des relevés expérimentaux," *Manuels de calculs techniques*, Editions Gauthier-Villars, Paris, 1962.

[23]Patankar, S.V. and Spalding, D.B., *Heat and Mass Transfer in Boundary Layers*, 2nd Edition, Intertext Book, London, 1970.